



CFD Contribution for the Investigation of a UAV Aerodynamic Performances Using the Spalart-Allmaras Turbulence Model

Z. Imine*, M. Senouci, T. Yahiaoui, S.M.A. Meftah

Aeronautics and Propulsive Systems Laboratory. Faculté de Génie Mécanique Université des Sciences et de la Technologie D'Oran Mohamed BOUDIAF BP1505 El M'nouar 31000 Oran Algérie.

*Corresponding author. imine_zakaria@yahoo.fr

Received. June 13, 2021. Accepted. July 27, 2021. Published. December 22, 2021.

DOI: <https://doi.org/10.58681/ajrt.21050204>

Abstract. In this paper, a numerical simulation of a turbulent flow around a UAV is performed. Different angles of incidence were used to evaluate aerodynamic performance. The Navier-Stokes equations are closed using a Spalart-Allmaras turbulence model. The results of the current numerical investigation were in good agreement with those found in the literature. Variations in lift and drag allow us to determine the total take-off weight and effective power required to move this UAV in various flight configurations (take-off, cruise flight, and landing). The contours of the total pressure around the UAV have been determined to have a preliminary observation on the parts of the UAV most in demand by the dynamic pressures.

Keywords. CFD, Turbulence, Performances, Lift, Drag, Incidence.

INTRODUCTION

A fixed-wing UAV, also known as a UAV (Unmanned Aerial Vehicle), is a small aircraft that can fly autonomously with only a virtual pilot on board. This does not imply that the plane is completely out of control as it leaves the runway. The presence of a human being in the control boucle is important. However, the command operator is positioned on a base station, either on the ground, at sea, or in a control station. He may intervene at any time to assess the situation, review the engagement rules, and, if necessary, halt the mission. The design of a UAV has been developed in a variety of research laboratories around the world. Military personnel was among the first to initiate such projects. Indeed, many countries' militaries tend to deploy UAVs into high-risk areas rather than sending soldiers to carry out observation and

war operations. This type of flying engine can perform a range of activities, ranging from scientific experiments to detection during the day or night.

In the field of aerodynamics, computational fluid dynamics is a key research tool that is being seen as a viable solution to wind tunnel tests. The question of whether the field of aerodynamics is purely theoretical or numerical has been raised by experts. They believe it is theoretical, owing to the many numerical tests used to compensate for the limitations of calculation methods (Ronzheimer, 2005). Alternatively, advances in computing power have made some CFD software more available and usable for non-linear fluid mechanics problems. In comparison to wind tunnel tests, the aerodynamic has been overdeveloped by its numerical component. The use of wind tunnel tests and CFD simulations leads to a perfect investigation of the flying machines' aerodynamic performance.

This paper aims to investigate a CFD contribution to a turbulent flow around a UAV. Aerodynamic performances are determined for different angles of attack. In addition, the presence and absence of landing gear in the UAV were the subject of two study configurations. The first step of this work is to build a solid UAV model with C.A.D (SolidWorks) software, which specifies its external geometry as shown in figure 1. To adapt its geometry to aerodynamic equations and test it under various flight conditions, this solid model is then exported to a mesh generation program (Flores et al., 1988). For estimates of the lift and drag coefficients in 40 meters/second, the CFD calculation code is used¹. The Spalart-Allmaras turbulence model (Li et al., 2000) is used to close Navier Stokes' transport equations to correctly predict the complex flow around the UAV particularly the stall region. A grid independence study is then performed to determine the accuracy of the calculation grid used for the CFD analysis.

UAV DESCRIPTION

This UAV as shown in figure 2 has a length of 2.68 meters and has a rectangular wing with a wingspan of 3.46 m. The airfoil is NACA 4415 with a chord of 0.5 m, which is fixed on the fuselage by an angle of 4° with neutral dihedral. The empennage group is a type of the letter H airfoil by NACA 0012 and attached to the wing by two beams, which also gives it the name of a bi-beams UAV. This one is characterized by remarkable stability at unacceptable roll axis moves and it is designed to have a pusher propeller that will be boarded behind the fuselage.



Fig.1. The solid model of the UAV.

¹ Bhaskaran R. FLUENT Short Course, <http://instruct1.cit.cornell.edu/courses/fluent> Includes step-by-step tutorials and problem sets. Chapters: Introduction to Computational Fluid Dynamics; Laminar pipe flow; Turbulent pipe flow; Compressible nozzle flow; Airfoil flow.

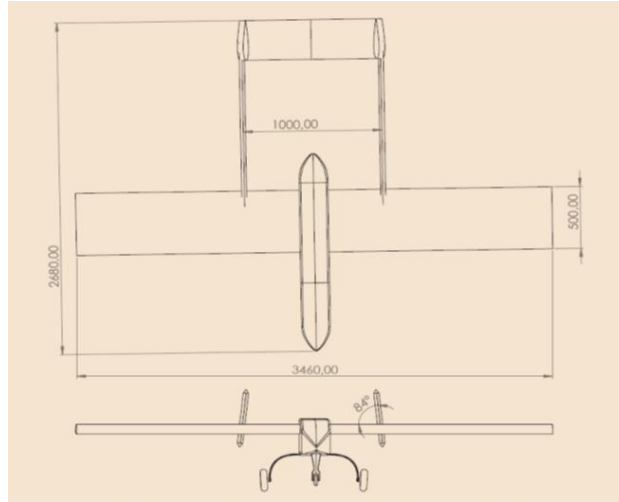


Fig.2. Description of this UAV.

FORMULATION OF THE PROBLEM

Transport equations and turbulence model

The flow around the aircraft is considered symmetric turbulent. The general forms of the transport equations are as follows:

Continuity equation

$$\frac{\partial}{\partial x_j} (\bar{\rho} \tilde{U}_j) = 0 \quad (1)$$

Equation of conservation of momentum

$$\frac{\partial}{\partial x_j} (\bar{\rho} \tilde{U}_i \tilde{U}_j) = \bar{\rho} g_i - \frac{\partial \bar{p}}{\partial x_i} - \frac{\partial}{\partial x_j} (\rho u_i'' u_j'') + \frac{\partial}{\partial x_j} \left[\mu \left(\frac{\partial \tilde{U}_i}{\partial x_j} + \frac{\partial \tilde{U}_j}{\partial x_i} \right) - \frac{2}{3} \mu \frac{\partial U_k}{\partial x_k} \delta_{ij} \right] \quad (2)$$

Turbulence model

The turbulence model used in this present work is a one transport equation model for the quantity suggested by Spalart-Allmaras (Benhamza and Belaid, 2009):

$$\frac{\partial(\rho v)}{\partial t} + \vec{\nabla} \cdot (\bar{\rho} \tilde{v}) = \vec{\nabla} \cdot \left[\frac{\mu + \rho v}{\sigma_{SA}} \vec{\nabla} \tilde{v} \right] + P_v - D_v \quad (3)$$

Or the terms of production and destruction are defined as follows:

$$P_v = C_{b1} C_\mu \tilde{S} \bar{\rho} \tilde{v} + C_{b2} \frac{\bar{\rho} (\tilde{v})^2}{\sigma_{SA}} \quad (4)$$

$$D_v = C'_{\omega 1} f_\omega \frac{(\bar{\rho} \tilde{v})^2}{\bar{\rho} d^2} \quad (5)$$

With

$$f_x = g \left(\frac{1 + C_{\omega 3}^6}{g^6 + C_{\omega 3}^6} \right)^{1/6} \quad / \quad g = r + C_{\omega 2} (r^6 - r) \quad (6)$$

And

$$M_t = \bar{\rho} \tilde{v} \frac{\chi^3}{\chi^3 + C_{v1}} \quad / \quad \chi = \frac{\bar{\rho} \tilde{v}}{\mu} \quad (7)$$

And the closing coefficients are given by the following values:

$$\sigma_{SA} = \frac{2}{3}; \quad C_{b1} = 0.1355; \quad C_{b2} = 0.622$$

$$C_{v1} = 7.1; \quad C_{\omega1} = 0.3; \quad C_{\omega3} = 2 \quad (8)$$

(For more information see reference (Benhamza and Belaid, 2009))

RESULTS AND DISCUSSION

In this study and to obtain the maximum of information for the two UAV configurations, several angles of attack were considered from -9° to 45° with an increment of 3° and with a velocity at infinity equal to 40 m/s

The longitudinal distribution of UAV's transversal sections is a way of visualizing large pressure variations that disrupt the flow, causing turbulence and a lot of drag. As you can see in Figure 3, the cross-sectional design of the present UAV results in an almost perfect surface rule distribution reflecting the section distribution of bi-beam UAVs. This means that instead of having pressure fluctuations as the flow moves around and along with UAV, the pressure increases smoothly and decreases smoothly. This minimizes any turbulence and further reduces drag. Notice that there is a big jump in the cross-section where the fuselage merges with the wing at the leading edge and similarly a big drop at the trailing edge. However, a near-zero distribution is observed at the level of the beams followed by another increase and decrease at the level of the tail.

In Figure 4, the distribution of the cross-sections of the present UAV and that of the Shadow RQ-7A is shown (Drab, 2012). As you can see, there is a great similarity between the two UAVs except for the shape of the two tail units. The widest part of the fuselage is in the same longitudinal position as the wing. This UAV has a narrower fuselage than the RQ-7A, resulting in a minimum cross-section of around 25%. This design is adopted so that it can quickly squeeze through the air without having to move as much air as the RQ-7A.

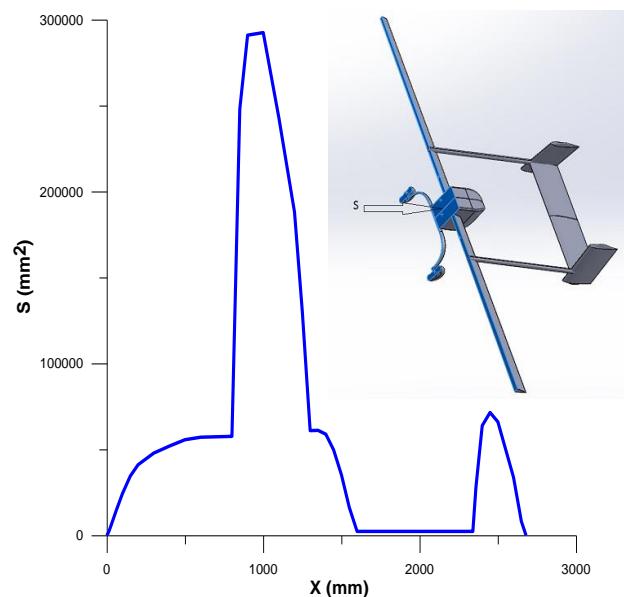


Fig.3. The longitudinal distribution is cross-sectional of the present UAV.

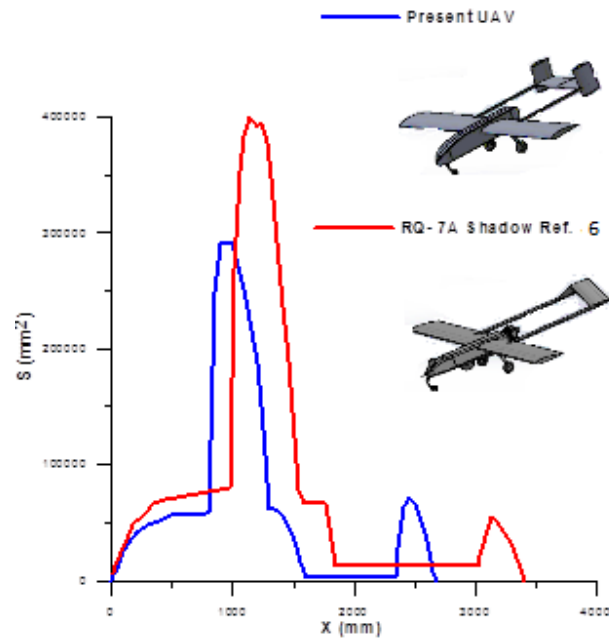


Fig.4. The longitudinal distribution cross-sectional comparison.

Figure 5 shows the evolution of the lift coefficient as a function of the incidence angles for the two UAV configurations. In general, the two curves look the same except that the configuration with the landing gear is slightly overlapped with the one without the landing gear. In the two curves, we observe that the lift increases almost linearly between the incidence of -9° and 27° as predicted by the literature (Meftah et al., 2011). The stall is carried out at 27° for a maximum lift coefficient of around 1.3. The curve also indicates that at 0° of incidence angle the lift coefficient C_l equals 0.3. This makes sense because our UAV has non-symmetrical airfoil wings. The zero-lift angle corresponds to -8° below this angle and negative lift occurs.

Figure 6 represents the drag coefficient as a function of the angle of incidence. Also, we note that the two curves have the same shape except that the configuration with landing gear is slightly superimposed compared to that without landing gear because the presence of the landing gear generates a small additional drag. For zero incidence, the drag coefficient is $C_d = 0.05$. This low value seems reasonable due to the tapered and aerodynamic shape of the UAV. The drag coefficient increases with increasing incidence angles without there being a rupture zone. We also note that the two curves which represent the two configurations always have positive values and never intersect the axis of incidence.

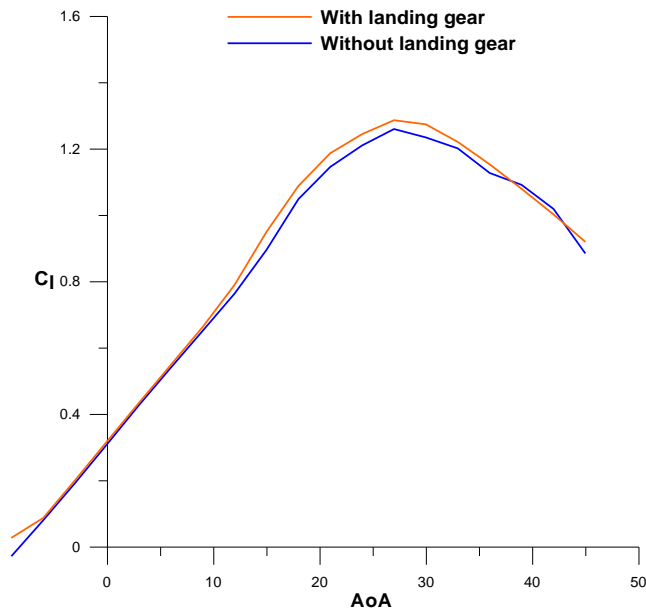


Fig.5. Lift coefficient for several angles of attack.

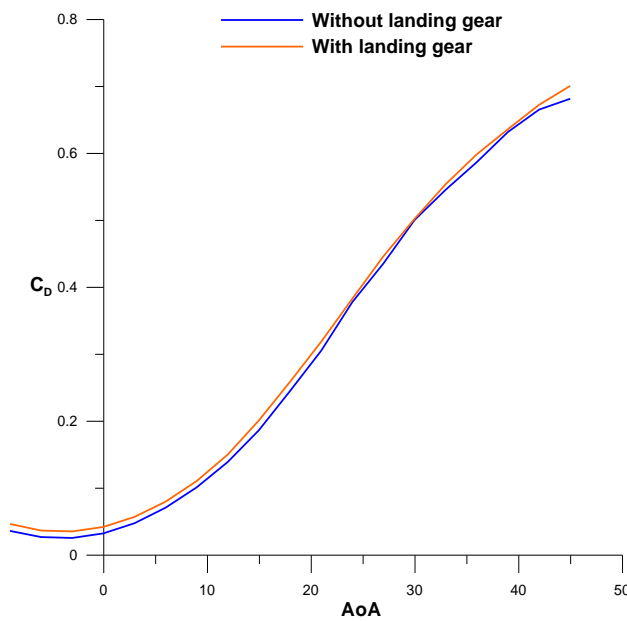


Fig.6. The drag coefficient for several angles of attack.

Figure 7 represents the pitching-moment coefficient C_m according to a different angle of attack, the curve indicates the increase of this coefficient with the increase of incidence angles up to around the value $i=33^\circ$, where the stall is realized. At this point, the pitching-moment coefficient begins to decrease slightly. The curve also indicates that at $i=0^\circ$ the pitching-moment coefficient is not zero and equal to 0.22 and this value is an expected result view of the asymmetrical airfoil of the wings.

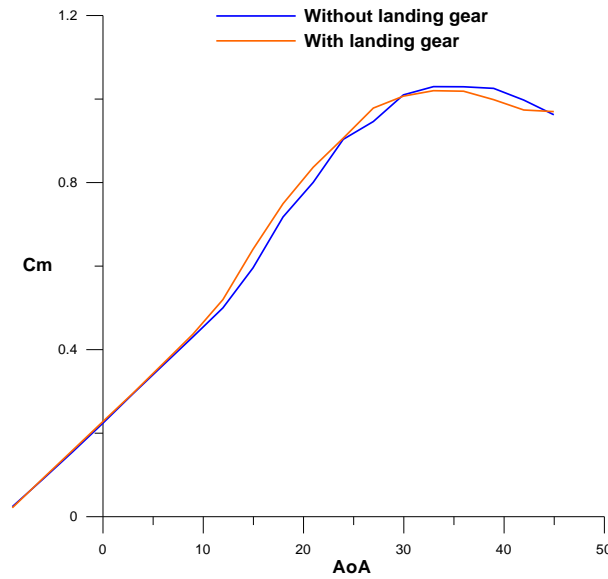


Fig.7. Pitching-moment coefficient for several angles of attack.

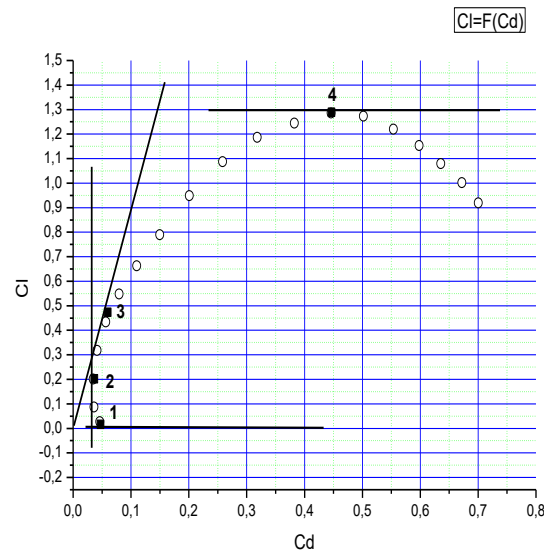


Fig.8. Polar of UAV with the landing gear.

To better develop the characteristics of the airfoil used in this UAV, the plot of the polar which represents the function $C_l = f(C_d)$ is very important to determine the characteristic points of different phases of UAV flight. Figure 8 shows the characteristic points of the polar of this UAV:

1. For zero lift C_{l0} : Obtained at an angle of incidence $i = -8^\circ$;
2. For a minimum drag $C_{d \min} = 0.022$ Obtained at an angle of incidence $i = -4^\circ$;
3. For a maximum fineness of $f_{\max} = 8$ Obtained at an angle of incidence $i = 0^\circ$;
4. For maximum lift $C_{l \max} = 1.3$ Obtained at an angle of incidence $i = +27^\circ$.

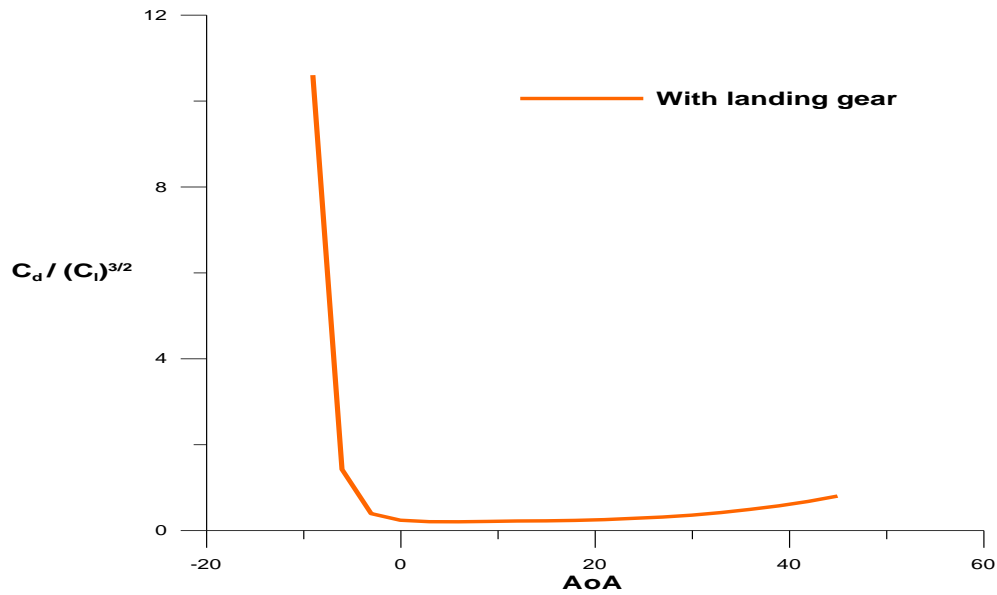
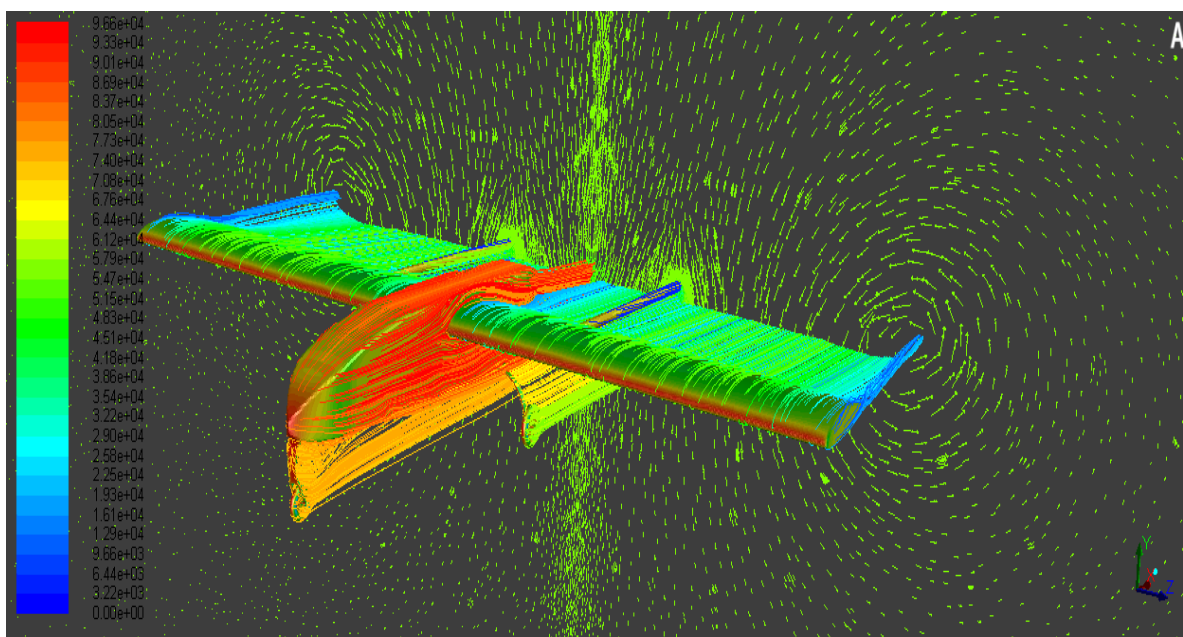


Fig.9. Minimum descent rate factor for several angles of attack.

A failure of propulsion (engine failure) where the UAV is faced with hovering and holding air for as long as possible is characterized by determining the minimum of the factor $C_d / C_l^{3/2}$ as a function of the angle of attack. However, we see in Figure 9 that the term $C_d / C_l^{3/2}$ takes a minimum value for an angle of attack of the order of $i = 6^\circ$ and which corresponds respectively to $C_l = 0.54$ and $C_d = 0.079$.

Figures 10a, b, and c show the streamlines and the velocity vectors of the wake flow respectively for several angles of attack $i = 0^\circ$, 9° , and 27° . We note that the contribution of the CFD manages to capture the wingtip vortices, which form in counter-rotating cyclones even for a cruising incidence of $i = 0^\circ$ and which generate a loss of lift due to induced drag. Also, we note the presence of air streams stuck to the wing upper in the direction of the flow which confirms at such an incidence the boundary layer separation is not expected.



(a) AoA = 0°

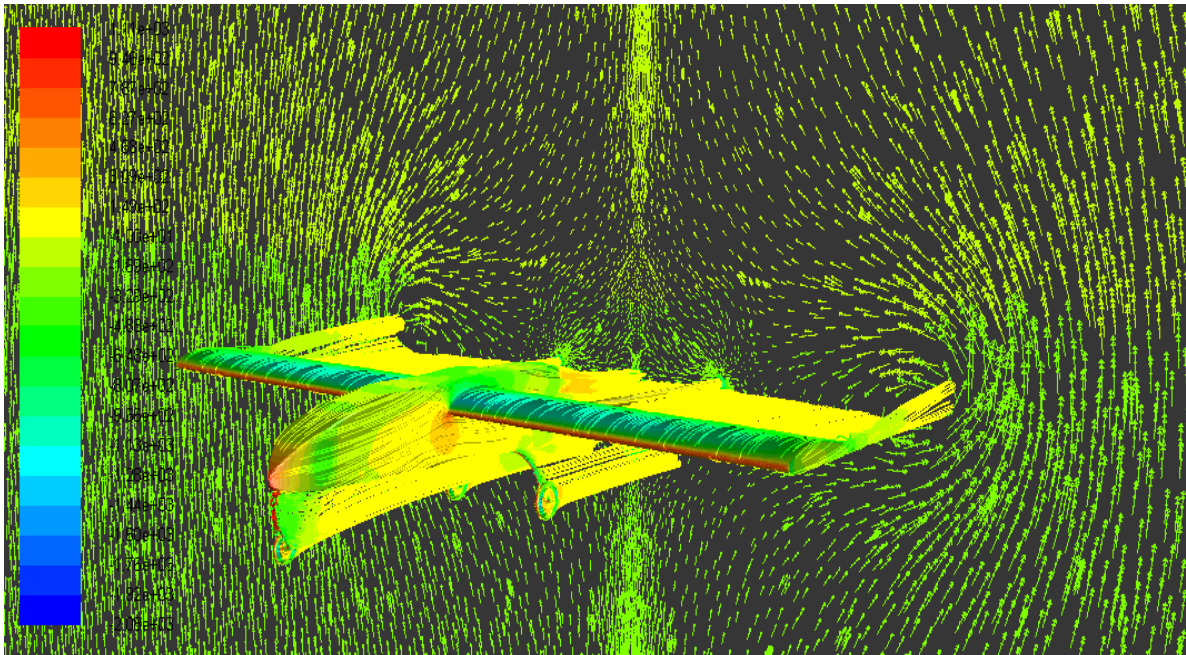
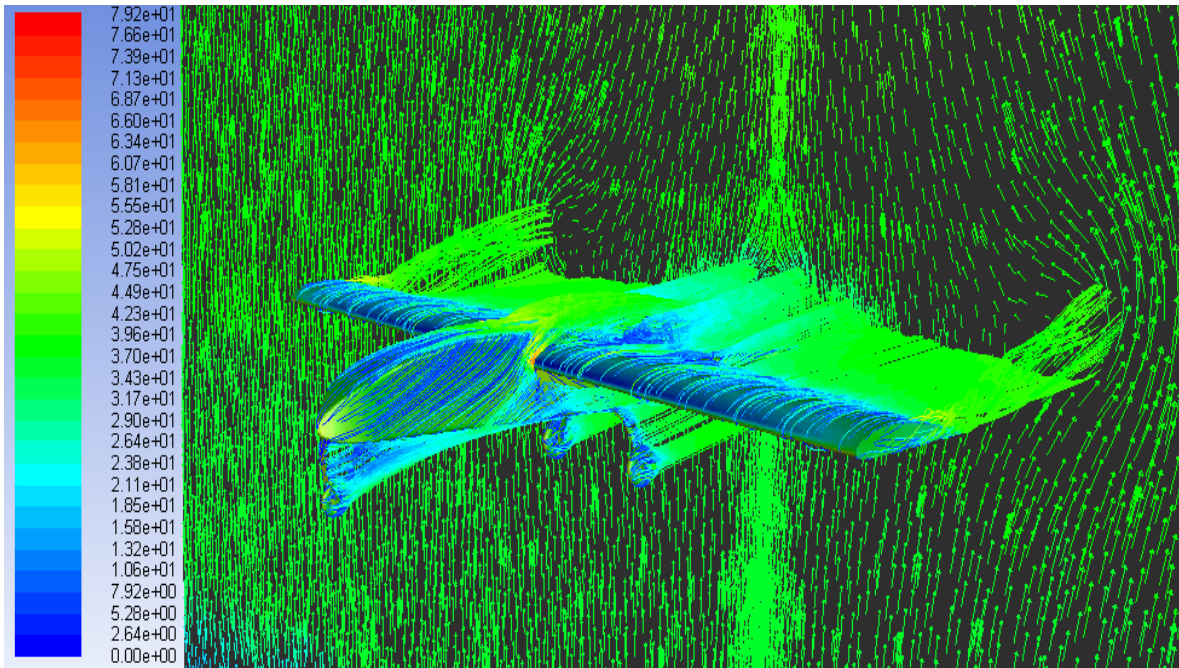
(b) $AoA = 9^\circ$ (c) $AoA = 27^\circ$

Fig.10. Streamlines and velocity vectors for several angles of attack.

Figures 11a, b and c represent the distribution of the total pressure around the UAV for the following attack angles $i = 0^\circ$, 9° , and 27° . It was noticed that in figures 11.b and 11.c that there is a decrease in pressure on the upper of the wing (blue color) while the pressure on the lower increases (red color) as the angle of attack increases to the point of stall.

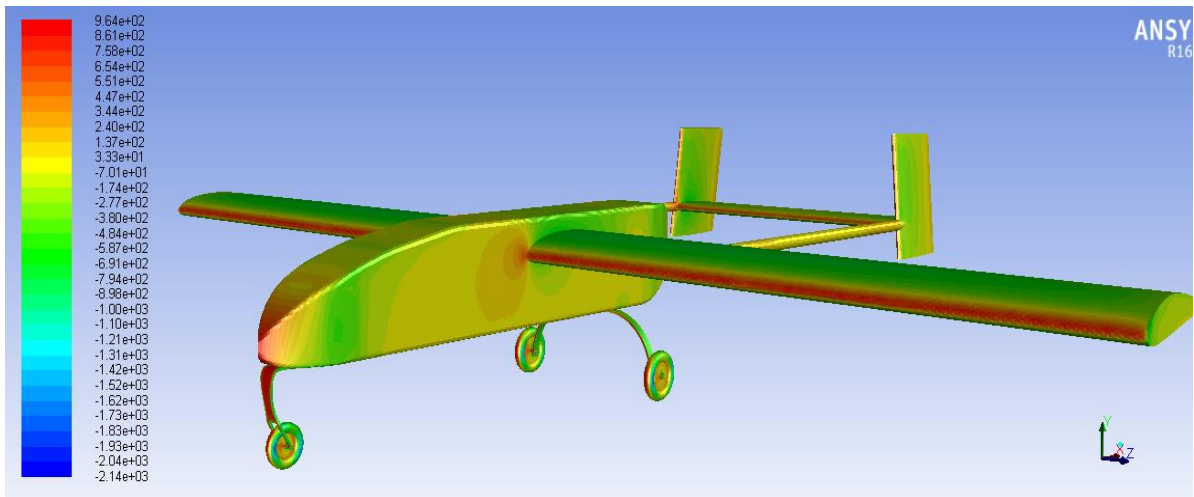
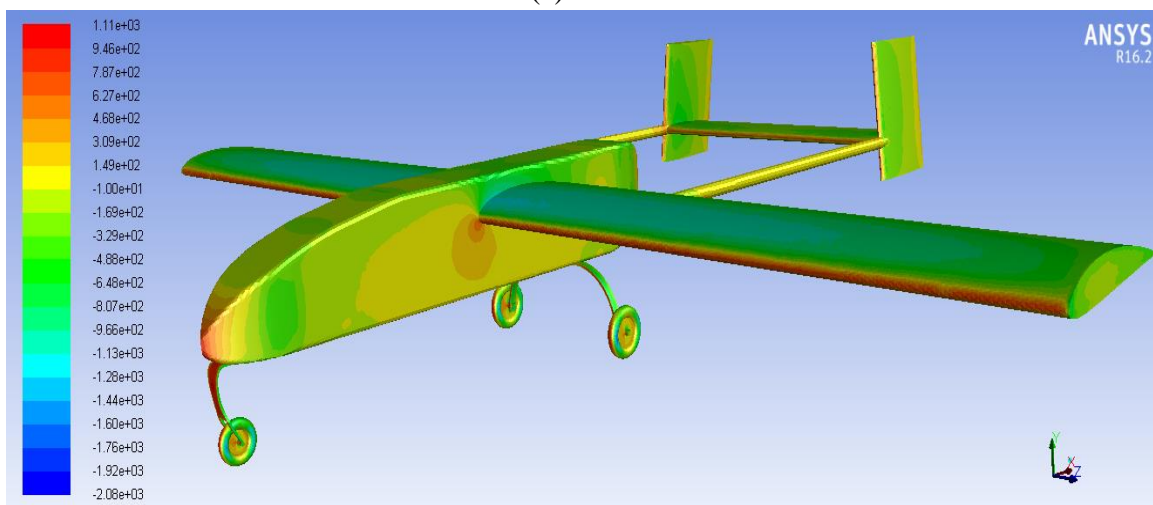
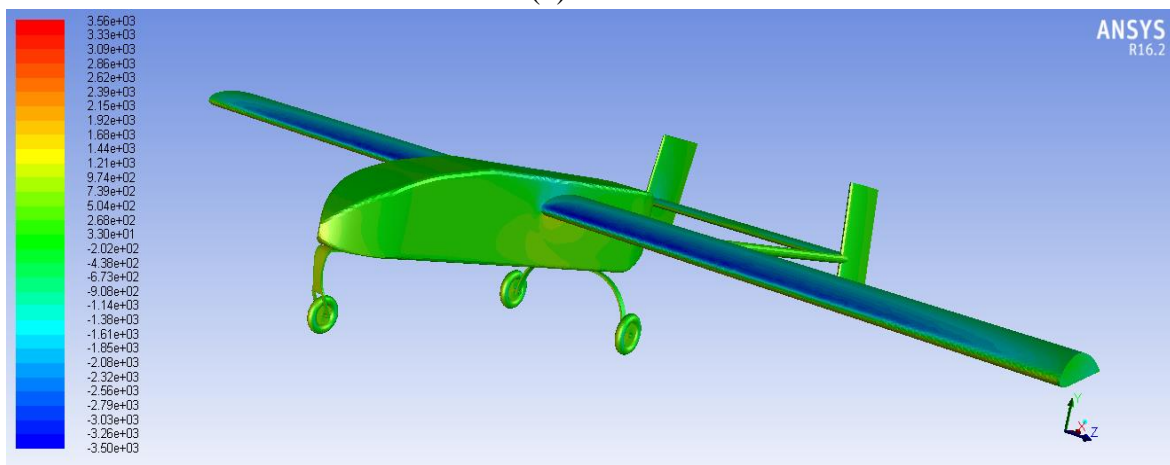
(a) $\text{AoA} = 0^\circ$ (b) $\text{AoA} = 9^\circ$ (c) $\text{AoA} = 27^\circ$

Fig.11. Static pressure contours for multiple angles of attack.

CONCLUSION

In the present paper, a numerical investigation is presented to evaluate the aerodynamic performance of a UAV such as the coefficients of lift, drag, and moment. The model obtained from computer-assisted drawing software was exported to the pre-processor for mesh

generation. CFD software based on the finite volume method was used to simulate the motion of a UAV in a turbulent atmosphere for possible aerodynamic design.

The aerodynamic performances are determined according to several angles of attack which vary between $[-9^\circ, 45^\circ]$ with an increment of three degrees to collect the maximum information for a velocity at infinity equal to 40 m / s. In addition, to better predict all the phenomena of stationary and turbulent external flows, the Spalart-Allmaras is used for the closure of the Navier-Stokes equations.

The results obtained by the present numerical investigation showed a good agreement with those encountered in the literature. The variations in lift and drag allow us respectively to assess the total take-off weight and the useful power for the displacement of this UAV for different flight configurations (take-off, cruising flight, and landing). The contours of the total pressure around this UAV were determined to have a preliminary observation on the parts of the UAV most stressed by the dynamic pressures.

REFERENCES

- Benhamza, M. E., & Belaid, F. (2009). Computation of turbulent channel flow with variable spacing riblets. *Mechanika*, 79(5).
- Drab O. http://olive-drab.com/uav_rq7 Archived from the originale on 15 May 2012. Retrieved 15 May 2012.
- Flores, J., Reznick, S. G., Holst, T. L., & Gundy, K. (1988). Transonic navier-stokes solutions for a fighter-like configuration. *Journal of Aircraft*, 25(10). <https://doi.org/10.2514/3.45674>
- Li, J., Li, F., Qin, E., Li, J., Li, F., & Qin, E. (2000). Numerical simulation of transonic flow over wing-mounted twin-engine transport aircraft. *Journal of Aircraft*, 37(3). <https://doi.org/10.2514/2.2621>
- Meftah, S. M. A., Imine, B., Imine, O., & Adjlout, L. (2011). Numerical simulation of a flow around an unmanned aerial vehicle. *Mechanika*, 17(2). <https://doi.org/10.5755/j01.mech.17.2.339>
- Ronzheimer, A. (2004). Post-parametrization of CAD-geometries using freeform deformation and grid generation techniques. In *New Results in Numerical and Experimental Fluid Mechanics IV: Contributions to the 13th STAB/DGLR Symposium Munich, Germany 2002* (pp. 382-389). Springer Berlin Heidelberg.